ACS Catalysis

Research Article

pubs.acs.org/acscatalysis

Partial Oxidation of Methane to Methanol Using Bismuth-Based Photocatalysts

Sebastián Murcia-López,*[,†] Katherine Villa,[†] Teresa Andreu,*[,†] and Joan R. Morante[†,‡]

[†]Catalonia Institute for Energy Research (IREC), Jardins de les Dones de Negre 1, 08930 Sant Adrià de Besòs, Spain

[‡]Department of Electronics, University of Barcelona (UB), Marti i Franquès 1, 08028 Barcelona, Spain

ABSTRACT: Bismuth-based photocatalysts, Bi_2WO_6, $BiVO_4$, and coupled Bi_2WO_6/TiO_2−P25, have been synthesized by a facile hydrothermal method, characterized, and evaluated for the first time for the selective photooxidation of methane to methanol. Several conditions were used in order to better comprehend the reaction mechanism. The obtained $BiVO_4$ is, among the others, the most promising photocatalyst for this reaction, displaying higher CH_3OH selectivity and being more stable than the others. When Bi_2WO_6 was coupled with TiO_2, the methane conversion increased; however, overoxidation of CH_4 to CO_2 predominates. A similar effect is observed when electron scavengers such as O_2 or Fe^{3+} were introduced in the photoreactor as a result of the formation of highly oxidant radicals.

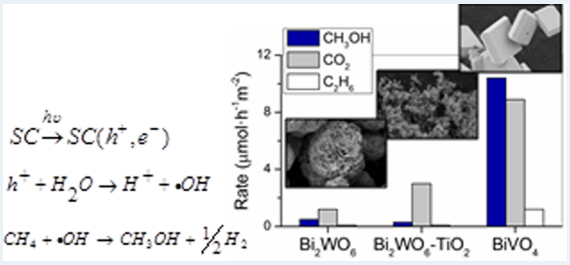

KEYWORDS: *photocatalysis, selective oxidation, Bi_2WO_6, $BiVO_4$, photo-Fenton*

1. INTRODUCTION

Nowadays, the development of new technologies for the direct conversion of methane into other products is an important challenge that has attracted much attention. As the main component of natural gas, methane is very abundant and possesses a high calorific power, so it is commonly used as direct fuel.[1] Besides this, the possibility of directly transforming methane into oxygenated products, such as methanol and formaldehyde, and even into longer chain compounds (e.g., ethane) also becomes an interesting alternative for its revalorization. Methanol, for instance, is a desirable product because it is an important chemical intermediate, used for obtaining other oxygenated compounds such as formaldehyde and acetic acid.[2] For these reasons, several efforts have been made in heterogeneous and homogeneous catalysis with diverse types of materials.[3,4] These studies, however, usually imply high temperatures and pressures or more complex systems, besides displaying poor selectivity associated with the continuous oxidation of methanol into CO and CO_2.

The photocatalytic processes allow promoting difficult reactions (even thermodynamically limited[1]) at mild conditions, by taking advantage of photoenergy instead of thermal activation. In this sense, photocatalysis arises as a promising alternative for the selective oxidation of methane into oxygenated products. Some approximations have been evaluated in literature, using several types of materials and oxidizers. From the evidence of the photochemical conversion of methane with water vapor at low temperature under certain irradiation conditions,[5] some authors have reported the photocatalytic oxidation of methane, mediated by semiconductors in the presence of H_2O. WO_3 has been one of the most commonly studied materials, mainly because of its lower band gap value, which makes it a good alternative in visible light processes. Initially, Taylor et al.[6,7] proposed the photocatalytic conversion of methane into methanol in a continuous process with La-WO_3 and UV light, at ∼90 °C. An electron scavenger (methyl viologen dichloride hydrate) and hydrogen peroxide as hydroxyl radical source were used in their studies. Later, Gondal et al.[8] also carried out the photoconversion of methane into methanol with WO_3, in a batch setup with a laser irradiation (visible light). Hydrogen peroxide and Fe^{3+} as electron scavenger were evaluated.

Besides WO_3, other kinds of materials as mesoporous silicas (V-containing MCM 41) and zeolites[9−12] have also been reported as photocatalysts for this reaction, by using NO and molecular O_2 as oxidizers. On the other hand, TiO_2, the most used semiconductor in photocatalytic applications, has attracted limited attention for this reaction. For instance Gondal et al.[13] have reported WO_3 as a better photocatalyst for methanol generation than rutile-TiO_2 and NiO. Other studies with Pt-TiO_2 materials, though, have been focused in steam reforming of methane (and methanol) for the generation of H_2 and CO_2.[14,15]

In recent years, bismuth-based materials have emerged as alternative photocatalysts to binary oxides as WO_3 and TiO_2. Specially considered for visible-light processes, it has been proposed that new hybridized band structures with Bi 6s and O 2p orbitals can be formed. Thus, besides a decrease in the band gap, the charge carrier mobility could be enhanced due to a less localized character of the s orbitals.[16] Among them, Bi_2WO_6

Received: June 12, 2014
Revised: July 18, 2014
Published: July 28, 2014

   dx.doi.org/10.1021/cs500821r | *ACS Catal.* 2014, 4, 3013−3019

and $BiVO_4$, with narrow band gaps (2.8 and 2.4 eV, respectively), have been two of the most studied oxides for different photocatalytic applications, like water splitting and pollutant degradation under visible light. For the latter, many efforts have been made for developing materials with controlled morphologies.[17−20] Despite being promising, only few reports deal with their application as photocatalysts in selective reactions,[21−23] besides some reports dealing with the CO_2 photoreduction into hydrocarbons with Bi_2WO_6 and $BiVO_4$.[24−26]

Moreover, to the best of our knowledge, these materials have not been yet evaluated in the selective photooxidation of methane to methanol. For this reason, in the present work, several bismuth-based materials have been studied for this reaction. At first, Bi_2WO_6 has been evaluated by changing some reaction conditions, including the addition of Fe^{3+} as electron scavenger. After this, given the possible drawbacks associated with the band configuration in this oxide, two additional materials have been synthesized: a coupled Bi_2WO_6/TiO_2−P25 system and $BiVO_4$, with expected more negative redox potentials in comparison to Bi_2WO_6. These materials have been characterized and evaluated under the best reaction conditions.

2. EXPERIMENTAL SECTION

2.1. Preparation of the Materials. Bi_2WO_6 was synthesized by following a procedure reported elsewhere.[27] Briefly, two solutions with the corresponding amounts of $Bi(NO_3)_3{\cdot}5H_2O$ and $Na_2WO_4{\cdot}2H_2O$ were prepared. The Bi precursor (0.005 mol) was dissolved in 5 mL of glacial acetic acid and the W solution (0.0025 mol) in 45 mL of Milli-Q water. These solutions were mixed to form a white suspension which was kept under stirring for 1 h. Then, this mixture was transferred to a Teflon liner inside a stainless steel autoclave and submitted to hydrothermal treatment at 140 °C for 20h. Finally, the precipitate was filtered, repeatedly washed, dried overnight, and calcined at 300 °C for 4h.

An analogous procedure was used for the preparation of $BiVO_4$. In this case, the vanadium precursor was anhydrous $NaVO_3$, which was added in a stoichiometric proportion (0.005 mol) to Bi.

The coupled Bi_2WO_6/TiO_2−P25 sample was synthesized with the same method. The corresponding amount of commercial TiO_2 (Evonik, P25) was added to the white suspension of Bi−W prior to the hydrothermal treatment, with a TiO_2/Bi_2WO_6 ratio of 50% wt. This material was named BW−Ti.

2.2. Characterization. The crystalline phase composition was estimated by X-ray diffraction (XRD), using a Bruker D8 Advance diffractometer equipped with a Cu Kα radiation (0.15417 nm) source, a LYNXEYE super speed detector and a Ni filter. Crystallite sizes of the different phases were determined from the line broadening of the corresponding XRD peaks by using the Scherrer equation.

BET surface area and porosity measurements were carried out by N_2 adsorption in a Micromeritics TriStar II instrument.

The morphology of the samples was observed in a Zeiss Auriga FESEM microscope.

2.3. Photocatalytic Oxidation Tests. For the photocatalytic oxidation of methane to methanol, a commercial photochemical reactor (Ace Glass) was used. This setup was equipped with an immersion medium-pressure mercury lamp (450W, Ace Glass) with UVC-visible radiation. Cold water was continuously recirculated through the inner jacket of the reactor, in order to control both the temperatures of the lamp and of the reaction system (~55 °C). The outlet gas tube was connected to a six port valve with a loop, used to allow the sample injection to a gas chromatograph (Shimadzu GC-2010, equipped with an Agilent J&W HP-PLOT Q column and TCD and FID detectors), in which the gas composition was analyzed.

During each test, a suspension of Milli-Q water (300 mL) with the corresponding amount of catalyst (1g/L) was added to the reactor and kept in suspension by mechanical stirring. A calibrated gas mixture of CH_4 in He (20%) was continuously sparged (~22.4 mL/min) through the reactor in the dark for 30 min, after which the illumination was turned on and a periodical injection of the outlet gas was made for the analysis of products.

In the additional tests with Fe^{3+}, $FeCl_3$ was used as salt precursor (1 mM), and 1 M H_2SO_4 was used to adjust the pH value to ~2.5. Then, the same amount of catalysts was added to the system, and the reaction was carried out following the procedure described above.

3. RESULTS AND DISCUSSION

3.1. Characterization. The XRD measurements of the different materials can be observed in Figure 1. In single

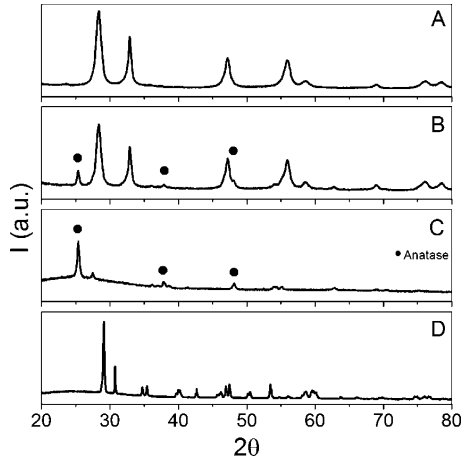

Figure 1. XRD patterns of: (A) Bi_2WO_6, (B) BW−Ti, (C) TiO_2−P25, and (D) $BiVO_4$.

Bi_2WO_6, only peaks corresponding to the russellite orthorhombic phase (JCPDS 39-0256) are seen. Some small peaks related to the anatase phase (JCPDS 21-1272) are also present, when this material is coupled to TiO_2−P25 as in the case of the BW−Ti sample. In this sense, the contribution of both single structures is evident.

In the case of the $BiVO_4$ sample, the pattern in Figure 1D corresponds to the scheelite monoclinic phase (JCPDS 14-0688), which has been usually described as the most photoactive in comparison to the tetragonal phases.[20,28,29]

The crystallite sizes calculated by using the Scherrer equation are collected in Table 1. Bi_2WO_6 and BW−Ti display similar sizes for the main russellite peak, with a small increment associated with the presence of TiO_2−P25. On the other hand, $BiVO_4$ presents the highest crystallite size. This fast growth of $BiVO_4$ particles when prepared by hydrothermal synthesis has been already reported in literature, having a particular influence on the surface area.[20]

dx.doi.org/10.1021/cs500821r | ACS Catal. 2014, 4, 3013−3019

Table 1. S_{BET} and Crystallite Size Values (Calculated from Scherrer Equation) for the Different Samples

sample	S_{BET} (m^2g^{-1})	crystallite size (nm)
Bi_2WO_6	30	8
BW−Ti	41	10
$BiVO_4$	2	28

The morphologies of the samples observed by SEM are presented in Figure 2. In this sense, there are important differences in the shapes and sizes of the different materials. Bi_2WO_6 (Figure 2A,B) displays an anisotropic growth in order to form nanoplates that self-assemble into 3D hierarchical structures through an Ostwald ripening process, as reported in previous works.[17] In the coupled BW−Ti system (Figure 2C), the presence of TiO_2−P25 during the hydrothermal treatment tends to inhibit the self-assembling mechanism. Thus, a heterogeneous morphology is obtained, with roundish particles that can be associated with TiO_2−P25 mixed with small nanoplates related to Bi_2WO_6. EDX analysis of this material indicates a final TiO_2/Bi_2WO_6 ratio of ca. 42%, more or less close to the nominal one. Finally, $BiVO_4$ (Figure 2D) consists of large irregular polyhedron of several sizes (1−2 μm), some of them with preferential exposure of (001) planes, suggesting also an anisotropic growth confirmed from the higher ratio of intensities between the (004) and the (121) peaks from XRD results.

In the case of single Bi_2WO_6, the difference between crystallite (estimated by the Scherrer equation) and particle sizes (seen by SEM) can be explained from the hierarchical growth, in which the large 3D structures are formed by smaller nanoplates.

The measurements of the BET area are displayed in Table 1. It is possible to observe that the coupled BW−Ti system exhibits the highest specific surface with an intermediate value between Bi_2WO_6 and TiO_2−P25 (~51 $m^2\ g^{-1}$), whereas $BiVO_4$ has the lowest one. From the point of view of the particle sizes, the values correspond well to the expected behavior among the four materials.

3.2. Photocatalytic Activity. *3.2.1. Blank Tests.* Prior to the photocatalytic tests, several blank tests without catalyst have been performed. In the test with only CH_4 under irradiation, no product was formed. Though, in the presence of water (300 mL), certain amounts of CH_3OH, CO_2, and C_2H_6 were observed under illumination. The corresponding conversion and selectivity results are presented in Table 2. Close to 2 μmol·h^{-1} of CH_3OH can be obtained after 120 min of irradiation. This process through a water photolysis mechanism in gas phase has been previously proposed by some authors,[5,7] as indicated in Scheme 1. In this case, under VUV light (at $\lambda \geq$ 185 nm), hydroxyl radicals can be produced from water photolysis and oxidize CH_4 into CH_3OH, through the formation of methyl radicals and their reaction with H_2O, as shown in eqs 2 and 3. Though, besides methanol, C_2H_6 can also be produced from the reaction between two methyl radicals as in eq 4, which differs from those results of Ogura and Kataoka, in which almost negligible combination of methyl radicals was observed.[5] This situation can be explained from the different used configurations, including the use of a different irradiation source. Finally, in addition to these two products, a relatively high amount of CO_2 was produced, indicating that some overoxidation process has taken place, through any of some potential oxidizing paths: direct oxidation with the nonselective ·OH radicals or through the formation of hydrogen peroxide or oxygen, as in eq 5.

3.2.2. Tests with Bi_2WO_6. Afterward, the photocatalytic process, which is represented in Scheme 2, was evaluated with Bi_2WO_6 under several reaction conditions. In this case, the irradiation of the semiconductor leads to the formation of hole−electron pairs in the valence and conduction bands, respectively. These holes (h^+) are able to initiate the hydroxyl radical formation by oxidizing adsorbed water onto the

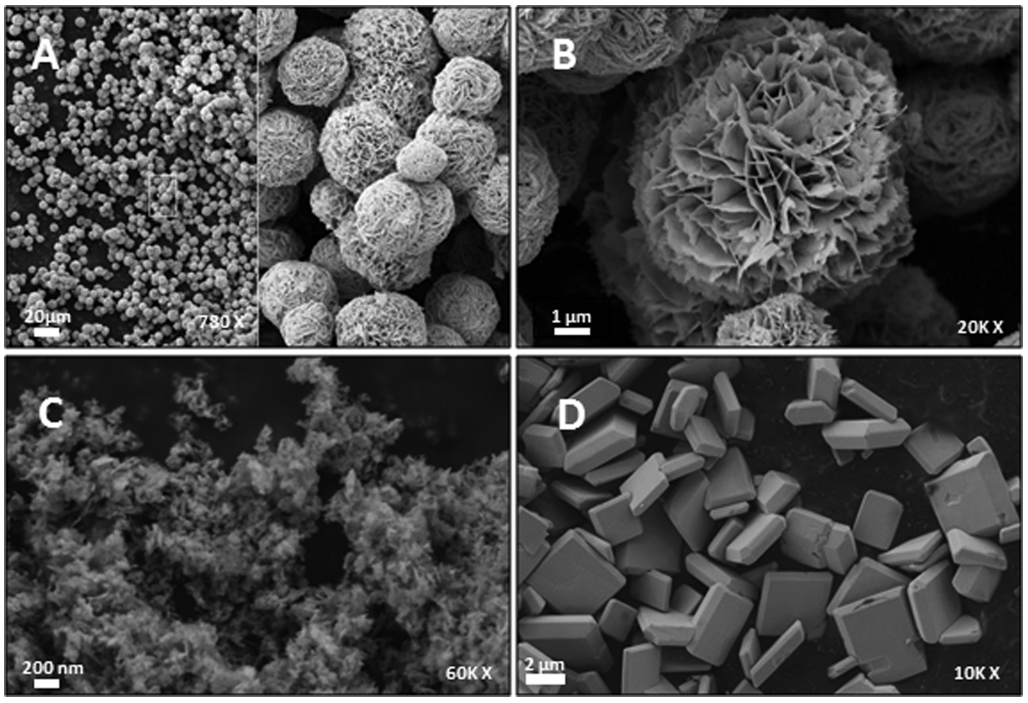

Figure 2. SEM micrographs of: (A, B) Bi_2WO_6, (C) BW−Ti, and (D) $BiVO_4$.

dx.doi.org/10.1021/cs500821r | ACS Catal. 2014, 4, 3013−3019

Table 2. Selectivity and Total Conversion Results after 120 min of Illumination during the Different Tests with and without Photocatalyst, at 55°C[a]

	selectivity (%)				
sample	CH_3OH	CO_2	C_2H_6	total conversion (%)	CH_3OH rate (μmol·h^{-1})
without catalyst (H_2O)	22.3	59.7	18.1	0.8 (0.8)	2.1
Bi_2WO_6	27.6	63.4	9.0	1.4 (1.6)	4.6

[a]In parentheses, the conversion values at 30 min.

Scheme 1. Photolytic Path

$$H_2O \xrightarrow{h\upsilon} \tfrac{1}{2} H_2 + \bullet OH \quad (1)$$

$$CH_4 + \bullet OH \rightarrow CH_3^\bullet + H_2O \quad (2)$$

$$CH_3^\bullet + H_2O \rightarrow CH_3OH + \tfrac{1}{2} H_2 \quad (3)$$

$$CH_3^\bullet + CH_3^\bullet \rightarrow C_2H_6 \quad (4)$$

$$\bullet OH + \bullet OH \rightarrow H_2O_2 \rightarrow H_2O + \tfrac{1}{2} O_2 \quad (5)$$

Scheme 2. Photocatalytic Path

$$SC \xrightarrow{h\upsilon} SC(h^+, e^-) \quad (6)$$

$$h^+ + H_2O \rightarrow H^+ + \bullet OH \quad (7)$$

$$H^+ + e^- \rightarrow H^\bullet \quad (8)$$

$$H^\bullet + H^\bullet \rightarrow H_2 \quad (9)$$

$$O_2 + e^- \rightarrow O_2^{\bullet -} \quad (10)$$

photocatalyst. The subsequent reactions for obtaining methanol and other products would be the same already represented in eqs 2−5 in Scheme 1.

At 55 °C, a CH_3OH rate of 4.6 μmol·h^{-1} was obtained with Bi_2WO_6 after 120 min, higher than the one obtained in the blank test without catalyst. Moreover, as seen in Table 2, the methanol selectivity increases at the expense of a decrease in that of ethane. This result suggests that the presence of the photocatalyst might be important in order to favor the reaction between methyl radicals and water, thus inhibiting their combination to produce ethane. From another point of view, the presence of the photocatalyst also enhances the methane conversion since the first 30 min of reaction, in comparison to the blank test.

Two additional tests were carried out with Bi_2WO_6 in order to determine the effect of different conditions. In the first one, the reaction temperature was increased to 90 °C, leading to a significant increase in the C_2H_6 formation (almost 3-fold), although CH_3OH was almost inhibited. This effect might be explained because of the expected higher amount of water vapor inside the reactor at this temperature, thus enhancing the photolytic formation of methyl radicals and their combination through reaction in eq 4. Hence, the decrease on the methanol rate is justified, as the ethane formation is a competitive reaction in which methyl radicals are consumed.

In the case of Bi_2WO_6, an important change in the color of the suspension was observed at the end of the tests. After a short time of exposure to air, the suspension easily recovers its original color, thus indicating this is a reversible process.

Besides the oxidation reactions through the holes, the reductive path through the concomitant electrons in the conduction band has also to be taken into account. For instance, if the semiconductor displays the proper band structure, it would be able to reduce water into H_2 (eqs 8−9). However, from the theoretical band structure proposed in literature for Bi_2WO_6, these processes are not expected to take place, as the electrons in its conduction band might not have the necessary redox potentials. The positions of the valence and conduction bands at pH = 0 for several materials are illustrated in Figure 3 (values extracted from literature[30−33]). It is important to keep in mind that as many aspects influence the solid−liquid interaction, different reported values can be found at varied conditions. In many cases, some variations might come, for instance, from differences in the estimated band gap values. Usually, calculations at several pH values are done by using the Nernst equation. Thus, more negative redox potentials can be expected at higher pH values (though the H_2O/H_2 potential would also be affected). Among the materials presented in Figure 3, $BiVO_4$ and TiO_2 have conduction bands closer to the potential for water reduction; therefore, from the thermodynamic point of view, they are more likely to evolve H_2 from H_2O, than Bi_2WO_6 and WO_3.

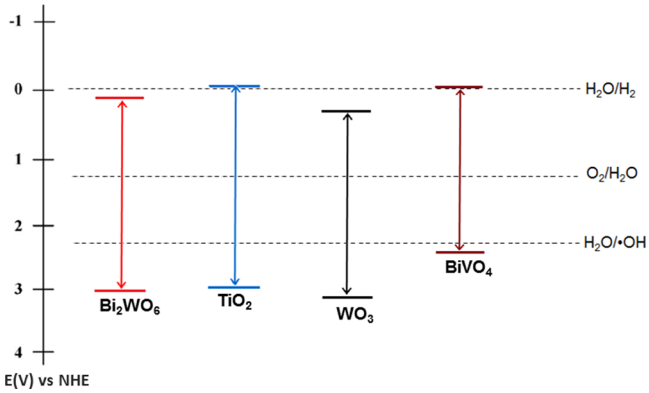

Figure 3. Conduction and valence bands positions for several materials at pH = 0, compared to some redox potentials. Some values were extracted from references.[30−33]

On the basis of the above considerations, the second additional test was performed with Bi_2WO_6 by continuously supplying O_2 into the system in order to elucidate the effect that this species may have as electron scavenger. In this case, the CO_2 production was greatly increased (almost 20-fold), being an important indicator of highly oxidizing conditions. On the opposite, C_2H_6 formation was completely inhibited, while CH_3OH rate was more or less similar to that obtained without O_2. Besides these results, it is important to point out that no change in the color of the suspension was observed at the end of the test. This is a qualitative indicator of the fact that some electron trapping must take place in the presence of O_2.

Even when no improvement in terms of methanol production is observed under these conditions, some

dx.doi.org/10.1021/cs500821r | ACS Catal. 2014, 4, 3013−3019

interesting aspects may arise from this test. Some authors have reported experimental and theoretical evidence about the thermodynamic drawbacks for the generation of superoxide radicals ($O_2^{\cdot-}$) with Bi_2WO_6 (eq 10).[34] However, additional reactions involving multielectron transfer to molecular oxygen have been proposed to occur in photodegradation processes with Bi_2WO_6. In fact, Sheng et al.[32] have recently found that H_2O_2 and ·OH radicals can be formed through multielectron reduction of O_2 with Bi_2WO_6, despite the expected lower rates associated with this kind of processes. In this sense, the formation of perhydroxyl radical ($HO_2^{\bullet}$) and H_2O_2 are more plausible than the direct formation of $O_2^{\bullet-}$, as these reactions have more positive redox potentials (E^0 $O_2/HO_2^{\bullet}$ = −0.05 V_{NHE}) and (E^0 O_2/H_2O_2 = +0.695 V_{NHE}), compared to the one-electron reduction of O_2 (E^0 $O_2/O_2^{\bullet-}$ = −0.33 V_{NHE}).[33] As it is well-known, H_2O_2 might act as the ·OH source. For this reason, its influence in the photooxidation of methane to methanol for systems with WO_3 has also been evaluated in literature, with more or less contradictory results: improvement in the CH_3OH to CO_2 ratio[7] or very oxidizing conditions in which CO_2 predominates overtime,[8] as in ours. Additionally, given the electron trapping associated with the O_2 presence (through any of the proposed mechanisms), a better charge separation can be expected, thus increasing the available holes for water and/or CH_3OH oxidation into other compounds and eventually CO_2.

An additional alternative that has not been mentioned is the generation of ozone via oxygen photolysis. As known, the VUV emission of 185 nm of the mercury lamp is able to dissociate O_2 into two $O^3(P)$ oxygen molecules, which could eventually generate O_3 by combining with other O_2 species,[35] and finally could dissociate with the 254 nm radiation of the mercury lamp, resulting in more O_2 and, eventually, H_2O_2 and ·OH radicals. However, this mechanism seems lees plausible from the point of view of our reaction conditions and would not be able to explain the nonreduction effect of the material in the presence of O_2.

It becomes clear in this sense that the presence of O_2 somehow enhances the oxidation process either by $O_2^{\bullet-}$ or H_2O_2 generation, by higher ·OH concentration or by increased availability of holes in the valence band. So, even when finding an alternative path in order to avoid the self-reduction of the material can be a good way for improving the photocalytic performance, the conditions must be carefully controlled in order to increase the CH_4 oxidation only to a certain extent. Hence, other approximation can rely on the direct substitution of the photocatalyst for others with different band structures. This possibility was also studied, and the results are presented below.

3.2.3. Fe^{3+} Addition. Given the evidence about the influence of the two concomitant paths in the photocatalytic process and the thermodynamic drawback associated with the reducing potential of materials as WO_3, different additives have been evaluated as electron scavengers in the literature. For this process in particular, methyl viologen dichloride (MV) and Fe have been reported to serve as electron-transfer agents in studies involving lanthanum-doped WO_3.[6] In the second case, the addition of Fe^{3+} seems to stabilize the methanol formation[8] through the capture of the photogenerated electrons in the conduction band in a process involving the Fe^{3+}/Fe^{2+} pair, as indicated in Scheme 3. As it can be observed, besides the electron scavenging, additional hydroxyl radicals can be formed via a Fenton reaction with H_2O_2.[36,37] These radicals may further play an important role in the overall process, as will be shown later.

Scheme 3. Fenton and Photo-Fenton Paths

$$Fe^{3+} + e^- \rightarrow Fe^{2+} \quad (11)$$

$$Fe^{2+} + H_2O_2 + H^+ \rightarrow Fe^{3+} + {\bullet}OH + H_2O \quad (12)$$

$$Fe^{2+} + {\bullet}OH \rightarrow Fe^{3+} + OH^- \quad (13)$$

$$Fe^{3+} + H_2O \xrightarrow{h\nu} Fe^{2+} + {\bullet}OH + H^+ \quad (14)$$

On the basis of these considerations, two final tests were carried out by adding Fe^{3+} to the system: a blank and a photocatalytic test in the presence of Bi_2WO_6, under the same standardized conditions (55 °C, 1g·L^{-1} of catalyst, 1 mM Fe^{3+}, pH 2.5).

The obtained results are depicted in Figure 4. There, it is possible to observe an important increase in the CO_2 rate

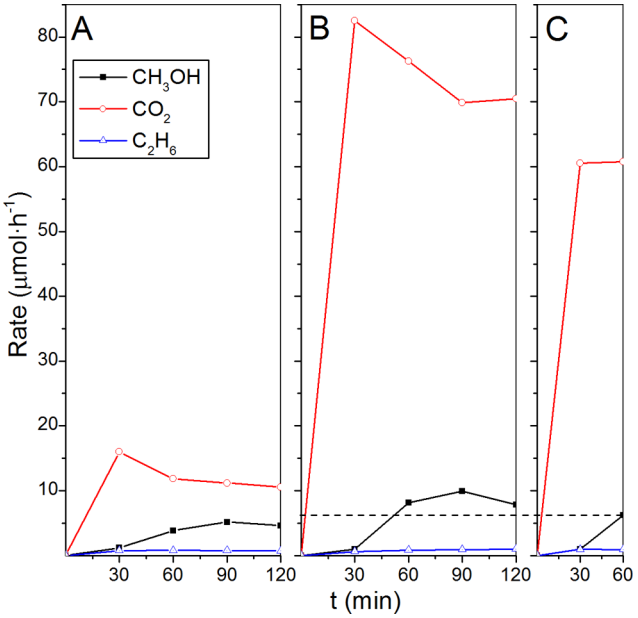

Figure 4. CH_3OH, C_2H_6 and CO_2 rates obtained during the different tests. Single Bi_2WO_6 (A), Bi_2WO_6 and Fe^{3+} (1 mM) as electron scavenger (B) and a solution of Fe^{3+} without photocatalyst (C).

(more than 5-fold), in comparison to the photocatalytic test without Fe^{3+}. These high rates indicate that very oxidizing conditions are reached, which could be explained from two aspects: the improved electron transfer from the conduction band of Bi_2WO_6 to Fe^{3+}, thus enhancing the charge separation, and the higher hydroxyl radicals concentration, able to overoxidise CH_4. Even when methanol rates are also increased, the presence of Fe^{3+} greatly affects Bi_2WO_6 selectivity to CH_3OH (below 10%), despite the significant increase in total conversion to ∼7%. It is important to point out that the conversion and selectivity estimation in these two tests with Fe^{3+} did not take into account an additional byproduct observed as a significant chromatographic peak that was not possible to identify among a wide series of organic compounds. Further analysis of this would be necessary for proper calculations. However, the measured rates in Figure 4 are not affected for this additional species.

From another point of view, it is interesting to observe that the coloration of the Bi_2WO_6 suspension seemed not to suffer

dx.doi.org/10.1021/cs500821r | ACS Catal. 2014, 4, 3013−3019

any change at the end of the test, suggesting that self-reduction is inhibited because of the Fe^{3+} presence.

On the other hand, in the blank test with a Fe^{3+} solution under the same reaction conditions revealed that solely Fe^{3+} in water (under illumination) is able to oxidize methane to CH_3OH, CO_2, and C_2H_6, in a similar manner to the photocatalytic tests. In this photo-Fenton process expressed through eq 14, hydroxyl radicals and Fe^{2+} are formed,[36] and methane is oxidized through the mechanism previously proposed.

3.2.4. Other Photocatalysts. Two additional materials were evaluated. First, a coupled system of Bi_2WO_6 and TiO_2–P25 was prepared as alternative, given the more negative conduction band of TiO_2–P25 in comparison to Bi_2WO_6, which could be better for water reduction to H_2, leading to an improved charge separation mechanism. This material was previously reported as a very active catalyst in a photodegradation process,[27] thanks to the intermediate features between the two single oxides and, probably, to the enhanced charge transfer from one material to the other, usually associated with this kind of coupled systems.[38,39] Second, a $BiVO_4$ sample prepared by very similar conditions to Bi_2WO_6, like other bismuth-based ternary oxides, with the advantage of exhibiting a conduction band with more reducing potential (as shown in Figure 3).

CH_3OH, CO_2, and C_2H_6 rates and selectivities after 120 min of illumination are depicted in Figure 5 for the three different

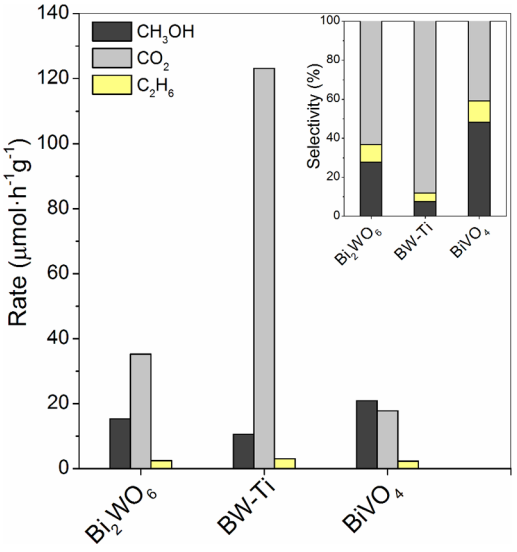

Figure 5. CH_3OH (A), CO_2 (B), and C_2H_6 (C) production rates with the different materials, at 55 °C.

materials. BW–Ti presented the highest CO_2 rates. This preferential formation of CO_2 at expense of the lowest CH_3OH rates is not unexpected, from the point of view of the reported results for this photocatalyst,[26] which exhibits a high oxidizing power that clearly exceeds those of Bi_2WO_6. The C_2H_6 levels are also higher with this sample, which could be expected if higher $CH_3\cdot$ concentrations are understood to come from more hydroxyl radicals formed through the process indicated in Scheme 2. Hence, the total conversion rises to ∼3.5%, but methanol selectivity decreases below 8%.

$BiVO_4$, on the contrary, displays an interesting behavior in comparison to the other photocatalysts. We observe not only an increase in the CH_3OH rate from ∼15 $\mu mol \cdot h^{-1} g^{-1}$ with Bi_2WO_6 to 21 $\mu mol \cdot h^{-1} g^{-1}$ but also lower CO_2 and C_2H_6 levels. Thus, despite showing a slightly lower methane conversion, the best CH_3OH selectivity is obtained with this material. At the end of the test, the suspension with $BiVO_4$ suffers a minimal change in the coloration, compared to the radical variation when using Bi_2WO_6. In this sense, the reversible reduction of the material might be much less pronounced with $BiVO_4$, as expected from its band structure. This fact may be confirmed by the differences in the total conversion between 30 and 120 min: a slight increase from 0.8 to 1.0% is found with $BiVO_4$, whereas the conversion seems to decrease from 1.6 to 1.4% with Bi_2WO_6.

Despite these results, the significant differences on the S_{BET} values among the samples have to be considered. Considerable differences would be obtained between the Bi_2WO_6-based materials and $BiVO_4$, if the product rates were normalized by surface area (as shown in the Graphical Abstract). This way, it is interesting to find that $BiVO_4$ is a good alternative as photocatalyst for this selective process despite its low S_{BET}. Designing and controlling textural and surface features during the preparation becomes an important challenge, in order to obtain materials with enhanced behavior.

In the particular case of methane to methanol photooxidation, these results demonstrate the importance of the two concomitant paths: oxidation and reduction, through both charge carriers. For this reason, the selection of a photocatalyst with the proper band configuration is crucial, unless some additives (as electron scavengers) are used. Besides this, a careful design and control of some features as the surface area is also important. This aspect would imply reaching a certain commitment degree with the crystalline growth.

4. CONCLUSIONS

Several bismuth-based materials were synthesized, characterized, and evaluated in the selective photooxidation of methane, with CH_3OH, CO_2, and C_2H_6 as the main products. Higher methane conversion and methanol selectivity were obtained in the photocatalytic test with Bi_2WO_6 than through the photolytic process with solely water. In presence of a continuous O_2 flow, very high CO_2 levels were obtained, because of the possible formation of oxidizing radicals as a consequence of electronic transfer from the conduction band of the photocatalyst to adsorbed O_2. When Fe^{3+} was added as electron scavenger, the total conversion was increased, given an enhanced charge separation and a major generation of hydroxyl radicals via Fenton and photo-Fenton mechanisms. However, despite the increased CH_3OH rates, CO_2 was the main product because of the highly oxidizing conditions.

$BiVO_4$ presented the best combination of conversion and selectivity, even better than those of Bi_2WO_6, in spite of its lower surface area. Additionally, an important aspect derived from the results and related to the two redox processes, indicated that although Bi_2WO_6 tends to self-reduce and deactivate after certain extent due to its band structure, $BiVO_4$, which has a conduction band with more negative potential and thus higher probabilities of generating H_2 from H_2O, is not reduced during the test.

Finally, a coupled Bi_2WO_6/TiO_2–P25 system was evaluated, showing higher photoactivity, at the expense of an important increase in the CO_2 formation.

These materials emerge as interesting photocatalysts for this reaction. Additional strategies such as increasing the surface area, enhancing the electron transfer by using other electron scavengers unable to produce ·OH radicals, or coupling with

dx.doi.org/10.1021/cs500821r | ACS Catal. 2014, 4, 3013–3019

other semiconductors will need to be expplored as alternatives in future work.

AUTHOR INFORMATION

Corresponding Authors

*E-mail: smurcia@irec.cat. Tel.: (34) 933 562 615.
*E-mail: tandreu@irec.cat.

Notes

The authors declare no competing financial interest.

ACKNOWLEDGMENTS

This work was partially supported by the European Regional Development Funds (ERDF, FEDER Programa Competitivitat de Catalunya 2007-2013), Ministerio de Economía y Competitividad (CSD2009-00050), and the Framework 7 program under the project CEOPS (FP7-NMP-2012-309984).

REFERENCES

(1) Yuliati, L.; Yoshida, H. *Chem. Soc. Rev.* **2008**, *37*, 1592−1602.
(2) Periana, R. A.; Mironov, O.; Taube, D.; Bhalla, G.; Jones, C. *Science* **2003**, *301*, 814−818.
(3) Otsuka, K.; Wang, Y. *Appl. Catal. A* **2001**, *222*, 145−161.
(4) Reddy, P. V. L.; Kim, K. H.; Song, H. *Renew. Sust. Energy Rev.* **2013**, *24*, 578−585.
(5) Ogura, K.; Kataoka, M. *J. Mol. Catal.* **1988**, *43*, 371−379.
(6) Taylor, C. E.; Noceti, R. P. *Catal. Today* **2003**, *84*, 9−15.
(7) Taylor, C. E.; Noceti, R. P. *Catal. Today* **2000**, *55*, 259−267.
(8) Gondal, M. A.; Hameed, A.; Suwaiyan, A. *Appl. Catal. A* **2003**, *243*, 165−174.
(9) Hu, Y.; Nagai, Y.; Rahmawaty, D.; Wei, C.; Anpo, M. *Catal. Lett.* **2008**, *124*, 80−84.
(10) Hu, Y.; Anpo, M.; Wei, C. *J. Photochem. Photobiol., A* **2013**, *264*, 48−55.
(11) Sastre, F.; Fornés, V.; Corma, A.; García, H. *J. Am. Chem. Soc.* **2011**, *133*, 17257−17261.
(12) López, H. H.; Martínez, A. *Catal. Lett.* **2002**, *83*, 37−41.
(13) Gondal, M. A.; Hameed, A.; Yamani, Z. H.; Arfaj, A. *Chem. Phys. Lett.* **2004**, *392*, 372−377.
(14) Yoshida, H.; Hirao, K.; Nishimoto, J.; Shimura, K.; Kato, S.; Itoh, H.; Hattori, T. *J. Phys. Chem. C* **2008**, *112*, 5542−5551.
(15) Nomikos, G. N.; Panagiotopoulou, P.; Kondarides, D. I.; Verykios, X. E. *Appl. Catal. B* **2014**, *146*, 249−257.
(16) Belver, C.; Adán, C.; Fernández-García, M. *Catal. Today* **2009**, *143*, 274−281.
(17) Zhang, L.; Wang, H. L.; Chen, Z. G.; Wong, P. K.; Liu, J. S. *Appl. Catal. B* **2011**, *106*, 1−13.
(18) Shang, M.; Wang, W.; Ren, J.; Sun, S.; Zhang, L. *CrystEngComm* **2010**, *12*, 1754−1758.
(19) Xi, G.; Ye, J. *Chem. Commun.* **2010**, *46*, 1893−1895.
(20) Obregón, S.; Colón, G. *J. Mol. Catal. A* **2013**, *376*, 40−47.
(21) Zhang, Y.; Zhang, N.; Tang, Z. R.; Xu, Y. J. *Chem. Sci.* **2013**, *4*, 1820−1824.
(22) Zhang, Y.; Xu, Y. J. *RSC Adv.* **2014**, *4*, 2904−2910.
(23) Murcia-López, S.; Vaiano, V.; Sannino, D.; Hidalgo, M. C.; Navío, J. A. *Res. Chem. Intermed.* **2014**, DOI: 10.1007/s11164-013-1523-3.
(24) Cheng, H.; Huang, B.; Liu, Y.; Wang, Z.; Qin, X.; Zhang, X.; Dai, Y. *Chem. Commun.* **2012**, *48*, 9729−9731.
(25) Zhou, Y.; Tian, Z.; Zhao, Z.; Liu, Q.; Kou, J.; Chen, X.; Gao, J.; Yan, S.; Zou, Z. *ACS Appl. Mater. Interfaces* **2011**, *3*, 3594−3601.
(26) Mao, J.; Peng, T.; Zhang, X.; Li, K.; Zan, L. *Catal. Commun.* **2012**, *28*, 38−41.
(27) Murcia-López, S.; Hidalgo, M. C.; Navío, J. A. *Appl. Catal. A* **2012**, *423−424*, 34−41.
(28) Fu, Y.; Sun, X.; Wanga, X. *Mater. Chem. Phys.* **2011**, *131*, 325−330.
(29) Zhang, A.; Zhang, J. *Mater. Lett.* **2009**, *63*, 1939−1942.
(30) Ng, C.; Iwase, A.; Ng, Y. H.; Amal, R. *J. Phys. Chem. Lett.* **2012**, *3*, 913−918.
(31) Hill, J. C.; Choi, K. S. *J. Mater. Chem. A* **2013**, *1*, 5006−5014.
(32) Sheng, J.; Li, X.; Xu, Y. *ACS Catal.* **2014**, *4*, 732−737.
(33) Kim, J.; Lee, C. W.; Choi, W. *Environ. Sci. Technol.* **2010**, *44*, 6849−6854.
(34) Saison, T.; Gras, P.; Chemin, N.; Chanéac, C.; Durupthy, O.; Brezová, V.; Colbeau-Justin, C.; Jolivet, J. P. *J. Phys. Chem. C* **2013**, *117*, 22656−22666.
(35) Zoschke, K.; Börnick, H.; Worch, E. *Water Res.* **2014**, *52*, 131−145.
(36) Rincón, A. G.; Pulgarín, C. *Appl. Catal. B* **2006**, *63*, 222−231.
(37) Mest'ánková, H.; Mailhot, G.; Jirkovsky, J.; Krysa, J.; Bolte, M. *Appl. Catal. B* **2005**, *57*, 257−265.
(38) Shang, M.; Wang, W.; Zhang, L.; Sun, S.; Wang, L.; Zhou, L. *J. Phys. Chem. C* **2009**, *113*, 14727−14731.
(39) Colón, G.; Murcia-López, S.; Hidalgo, M. C.; Navío, J. A. *Chem. Commun.* **2010**, *46*, 4809−4811.